Supporting Information

In-situ conversion of metal (Ni, Co or Fe) foams into metal sulfide (Ni_3S_2, Co_9S_8 or FeS) foams with surface grown N-doped carbon nanotube arrays as efficient superaerophobic electrocatalysts for overall water splitting

Mingrui Guo, Abdul Qayum, Shun Dong, Xiuling Jiao, Dairong Chen and Ting Wang**

School of Chemistry& Chemical Engineering, National Engineering Research Center for Colloidal Materials, Shandong University
E-mail: t54wang@sdu.edu.cn; cdr@sdu.edu.cn

1. Materials

Nickel (II) nitrate hexahydrate ($Ni(NO_3)_2 \cdot 6H_2O$), ferric nitrate ($Fe(NO_3)_3 \cdot 9H_2O$), urea, and potassium hydroxide (KOH) were purchased from Sinopharm Chemical Reagent Co. Ltd. Thiourea was purchased from Tianjin Guangcheng Chemical Factory. Ni foams, Fe foams, Co foams with a thickness of 1.6 mm were purchased from Kunshan guangjiayuan electronic material Co. Ltd. Pt/C (20 wt % of Pt) was purchased from Alfa Aesar (China). All the reagents were of analytical grade and used as-received without further purification. Ultrapure water (18.25 MΩ) were used in all experiments.

2. Characterization

Powder X-ray diffraction (XRD) patterns were collected on a Rigaku D/Max 2200PC diffractometer with a graphite monochromator and Cu K_α radiation (λ= 0.15418 nm). Morphology and microstructure of the products were characterized by a transmission electron microscope (TEM, JEOL JEM-1011) with an accelerating voltage of 100 kV, a field emission-scanning electron microscope (FE-SEM, SU8010), and a high-resolution transmission electron microscope (HR-TEM, JEOL JEM-2100) with an accelerating voltage of 200 kV. The scanning transmission electron microscope (HAADF-STEM) images and the corresponding EDS mapping images were collected by Talos F200X operated at 200 kV. The X-ray photoelectron spectra (XPS) were recorded on a Thermo SCIENTIFIC ESCALAB 250Xi, and the Al K_α line was used as the excitation source. The thermogravimetric analysis (TGA) were operated on an STA449F3 Jupiter (NETZSCH) analyzer in air with a heating rate of 10 °C min^{-1}. The feature of the solid-liquid contact interface between catalysts and water were characterized by using a Kruss DSA10 optical contact angel system. The hydrogen and oxygen were collected and analyzed on gas chromatography (3420A, BeiFenRuiLi Co., Ltd).

3. Synthesis

Synthesis of the NSF and the NSF/CNT.

Ni foams were cleaned through sonication consecutively in concentrated HCl solution (3 M) and acetone for 3 times to remove the NiO_x layer on the surface, then the foams were washed with DI water and ethanol for 3 times. In a typical synthesis process, the pre-cleaned nickel foams were placed in a ceramic boat located at the center of a tube furnace, and an alumina boat containing 8 g thiourea was placed in the entrance of the furnace as the sources of carbon, sulfur and nitrogen. Before the furnace was heated, Ar (99.99 % in purity) were introduced into the tube furnace system with a flow rate of 100 sccm for 30 min to drive the air out from the tube. Subsequently, the tube was heated up to 900 °C with a heating speed of 10 °C min^{-1} and kept at that temperature for 1 h. The obtained NSF/CNT were allowed to be cooled to room temperature naturally. For NSF preparation, the tube was heated up to 600 °C instead of 900 °C with a heating speed of 10 °C min^{-1} and kept at that temperature for 1 h.

Synthesis of the FeSF and the FeSF/CNT .

Fe foams were used to replace Ni foams in the above reaction system to prepare the FeSF/CNT. The tube furnance was heated up to 1000 °C with a heating speed of 10 °C min^{-1} and kept at that temperature for 2 h. The obtained FeSF/CNT were allowed to be cooled to room temperature naturally. For FeSF preparation, the tube furnance was heated up to 600 °C instead of 1000 °C with a heating speed of 10 °C min^{-1} and kept at that temperature for 1 h.

Synthesis of CoSF and the CoSF/CNT.

Co foams were used to replace Ni foam in the above reaction system to prepare the CoSF/CNT.The tube furnance was heated up to 900 °C with a heating speed of 10 °C min^{-1} and kept at that temperature for 1 h. The obtained CoSF/CNT were allowed to be cooled to room temperature naturally. For CoSF preparation, the tube was heated up to 600 °C and kept at that temperature for 1 h.

Synthesis of NiFe-LDH on nickel foams.

NiFe-LDH were synthesized using a hydrothermal method.[1] $Ni(NO_3)_2 \cdot 6H_2O$ (0.5 mmol), 0.5 mmol of $Fe(NO_3) \cdot 9H_2O$, and 5 mmol of urea were dissolved in 36 mL deionized water and agitated for 0.5 h, the solution was transferred to a 50 mL autoclave with a piece of Ni foam inside. Then, the autoclave was heated up to 120 °C and kept at that temperature for 12 h. After the reaction, the obtained Ni foam with surface coating NiFe-LDH nanosheets was washed with deionized water and absolute ethanol for three times and vacuum-dried at 60 °C for 8 h.

4. Electrochemical measurements and the adhesive force estimated by the size of the gas bubbles

Electrochemical measurements are performed with a CHI 760E electrochemical analyzer (CH Instruments, Inc., Shanghai) in a standard three-electrode system, using the produced

products as the working electrode, a graphite rod and a Hg/HgO working as the counter electrode and the reference electrode, respectively. All tests were carried out in N_2-saturated 1 M KOH at room temperature. All the potential values measured were calibrated with respect to reversible hydrogen electrode (RHE) using the Nernst equation: $E_{vs\ RHE} = E_{vs\ Hg/HgO} + 0.095 + 0.059pH$. The reported current density is based on the geometrical area of the working electrode. Linear sweep voltammetry (LSV) data was measured with a scan rate of 5 mV s^{-1}. The long-term stability tests were performed using the constant current electrolysis method (J=100 mA). To accomplish the full water electrolysis, NSF/CNT were also used as both anode and cathode in a N_2-saturated 1.0 M KOH electrolyte (two-electrode configuration). To compare the performance of the NSF/CNT electrodes with the state-of-the-art catalysts, Pt/C powders were loaded on a nickel foam with a catalyst loading of 10 mg cm^{-2} for HER and NiFe-LDH on nickel foams was used for OER measurements. Electrochemical impedance spectroscopy (EIS) were made (in the frequency range of 100 kHz to 0.1 Hz) in 1 M KOH solution. The ECSA was estimated from the doublelayer capacitance (C_{dl}) charging curve using cyclic voltammetry in a small potential range of 0.1-0.2 V vs. Hg/HgO and the scan rates were 1-10 mV s^{-1}. The long-term stability tests were performed using the constant potential electrolysis method. The linear sweep voltammetry measurements were all 85% iR-compensated.

The calculation of turn over frequency (TOF).

$$TOF = \frac{j \times S}{N \times F \times n}$$

In the above equation, j stands for the current density (A cm^2), S is the electrode area (cm^2), N is the number of electrons transferred to evolve a molecule of product (for H_2, it is 2 and for O_2, it is 4), F is the Faraday constant (96485 C mol^{-1}) and n is the number of active metal atoms in the catalyst material (mol).

The bubble adhesion on a rough surface can be calculated by the following equation:[2]

$$F = f_s * F_a \quad \text{(Equation 1)}$$

The gas bubble adhesion on an aerophobic surface in electrolyte is similar to the water droplets on hydrophobic surfaces, where the Cassie-Baxter equation can be used to measure the aerophobic properties:[3]

$$\cos \alpha^* = -1 + f_s\ (\cos \alpha + 1) \quad \text{(Equation 2)}$$

In this equation, α is the apparent contact angle (CA), α* is the apparent CA on the rough solid surface, and f_s is the solid fraction of the contact area. Using this equation, the solid fraction of the contact area f_s can be calculated.

As shown in Equation 1, the adhesive force (F_a) of a bubble on an ideal solid surface, which is related to surface tension (γ), bubble radius (r), and contact angle (α) can be calculated using the following equation (Equation 3).[4]

$$F_a = \gamma 2\pi(r \sin\alpha)\sin\alpha \quad \text{(Equation 3)}$$

For a two-dimensional nanosheets coated electrode such as the NiFe-LDH, one-dimensional edge area are S=15nm*700nm=0.0105μm^2. Estimated from the SEM images, there are approximately 27 pieces of nanosheets on the surface (1μm*1μm), and the solid part of the contact area with the gas bubbles are these one-dimensional edges of the LDH nanosheets, which can be calculated as $f_s=(1/10^{-6})*27*0.0105\approx0.3$ (30 %).

For the NSF/CNT, the solid contact to the gas bubbles are zero-dimensional tip-points of the nanotubes, $S_2=3.14*0.35*0.35=0.38\mu m^2$. There are approximately 20 CNTs on the surface area of NSF/CNT electrode (20μm*20μm), the solid part of the contact area to the gas bubbles are extremely low, $f_s =1/(400*10^{-6})*20*0.38*10^{-6}\approx 0.02$ (2 %).

Supplementary Figures:

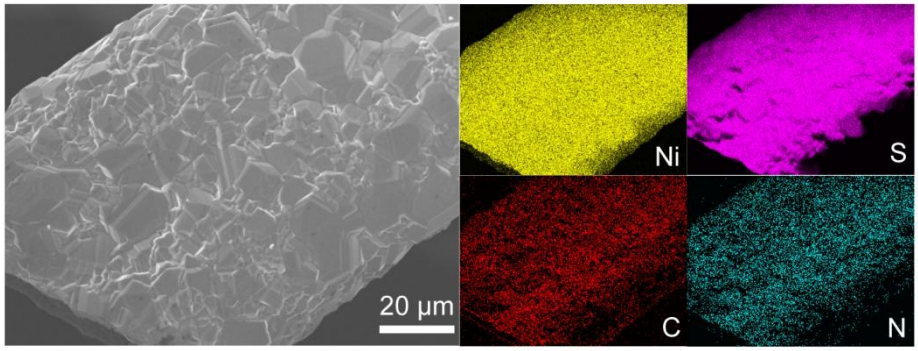

Figure S1. SEM and the corresponding elemental mapping images of the NSF obtained at 600 °C.

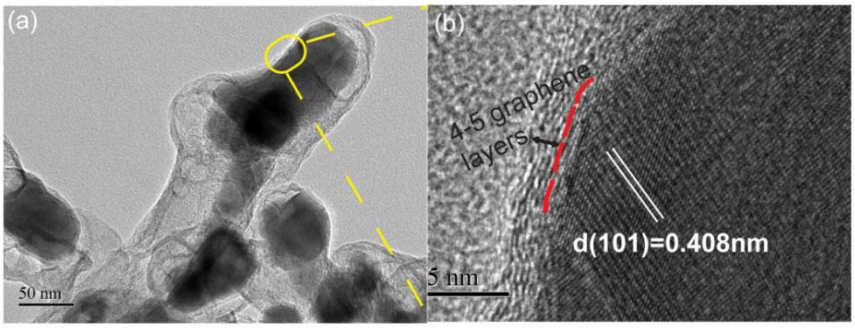

Figure S2. (a) TEM and (b) HRTEM images showing the tips of the carbon nanotubes in the NSF/CNT, the HRTEM shows the surfaces of the tips are covered by graphene layers and the fringes of the crystals are in corresponding to the Ni_3S_2 lattice.

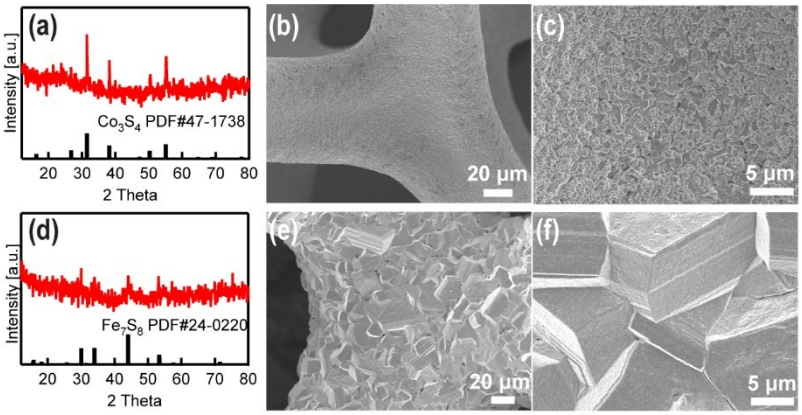

Figure S3. (a) XRD pattern, (b) low-resolution SEM and (c) high-resolution SEM images of the Co_3S_4 foams obtained at 600 °C; (d) XRD pattern, (e) low-resolution SEM and (f) high-resolution SEM images of the Fe_7S_8 foams obtained at 600 °C.

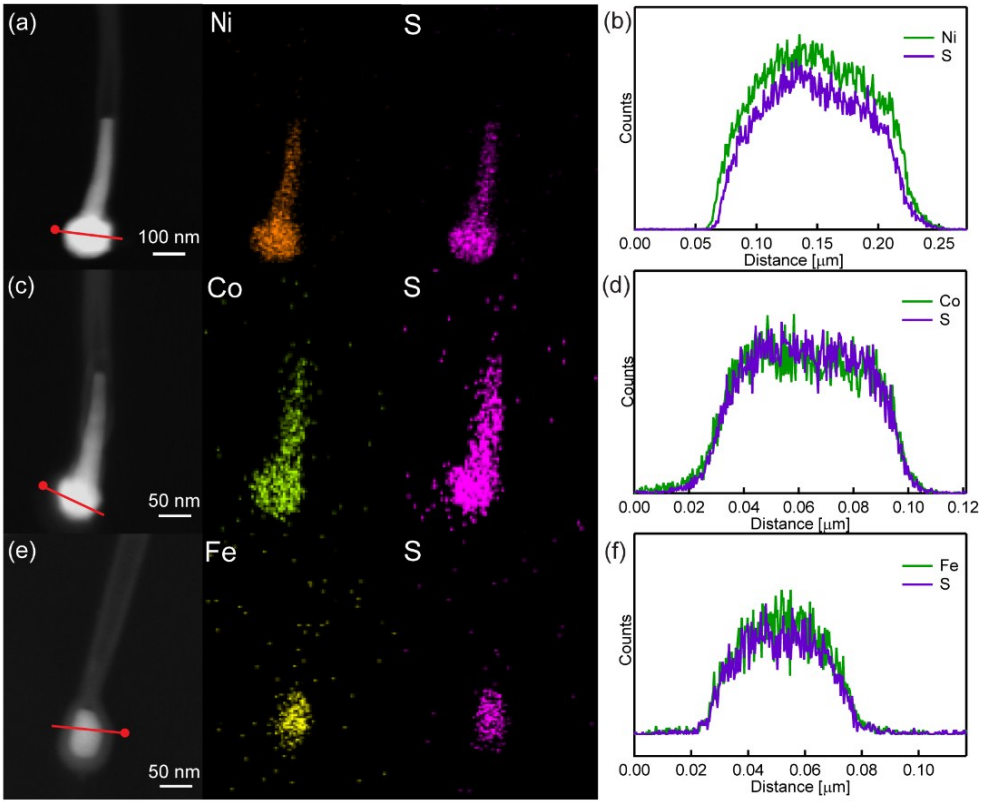

Figure S4. (a, c, e) STEM and the corresponding elemental mapping images of one tip of the carbon nanotubes catalyzed by nickel sulfide, cobalt sulfide and iron sulfide, respectively. (b, d, f) Line-scan STEM-EDS through the red line in (a, c, e) showing the distribution of the metal and sulfur elements.

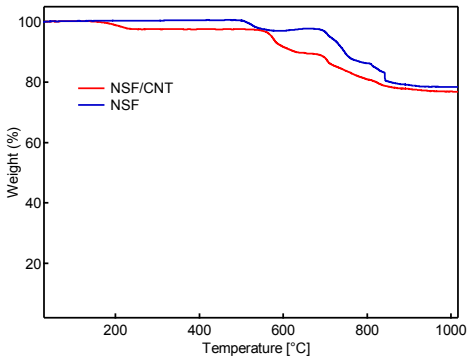

Figure S5. Thermogravimetric analysis (TGA) results measured in air in the temperature range from 25 to 1000 °C for NSF/CNT and NSF.

For NSF, the oxidation of the carbon coating on the sample surface occurs before 700 °C. The oxidation of NiS and their decomposition between 700-1000 °C resulted in a weight loss of ~19%. For NSF/CNT, the initial weight loss below 230 °C can be attributed to the removal of adsorbed water; the second step is before 700 °C with a weight loss of 8.6% is caused by the oxidation of surface carbon nanotubes. The weight loss of ~12% between 700-1000 °C can be attributed to the decomposition and the oxidation of Ni_3S_2.

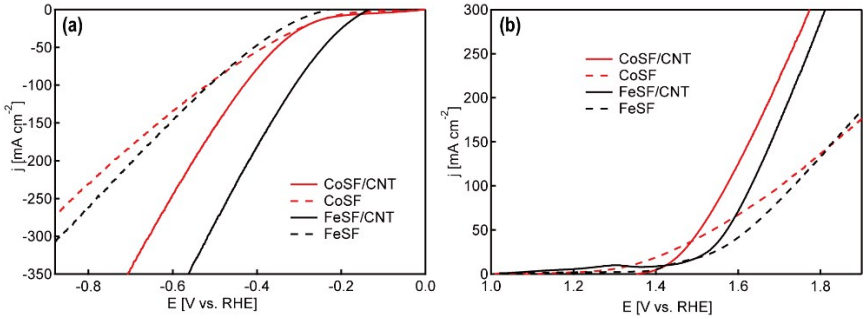

Figure S6. (a) LSV curves showing the enhancement of the HER performance after carbon nanotube coating. (b) LSV curves showing the enhancement of the OER performance after carbon nanotube coating.

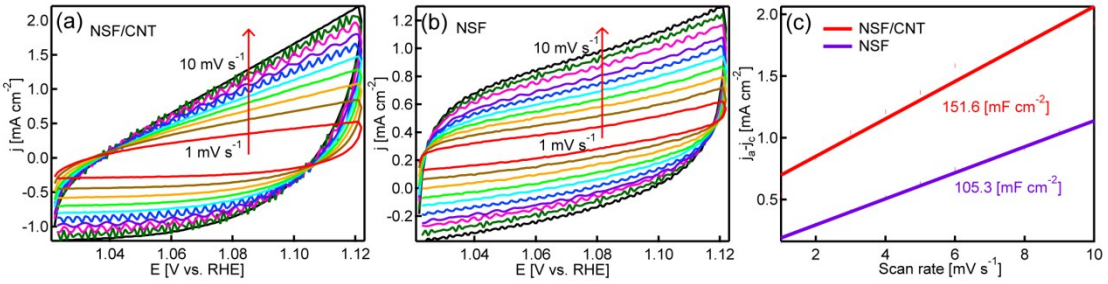

Figure S7. The CVs of the (a)NSF/CNT and (b) NSF catalysts with various scan rates under the non-faradic range versus RHE. (c) ECSA of the NSF/CNT and NSF.

Figure S8. EIS spectra of the NSF/CNT compared with the NSF. (a) Fitted parameters from the EIS plots. (b) The equivalent circuit used for fitting the EIS results.

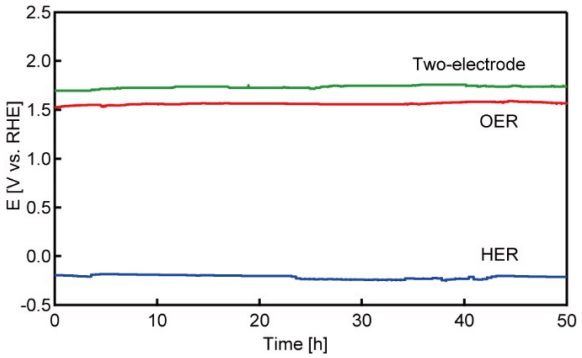

Figure S9. Long-term stability tests of the NSF/CNT as the working electrode for HER (blue line) and OER (red line) at a current of 100 mA. The green line shows the potential stability when using the NSF/CNT for both HER and OER in a two-electrode configuration.

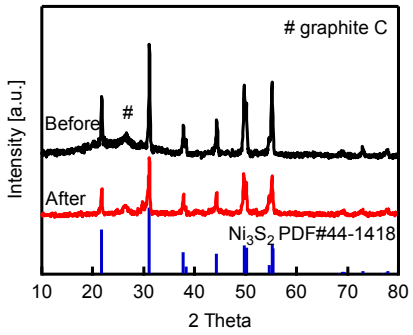

Figure S10. XRD patterns of NSF/CNT sample obtained before and after OER.

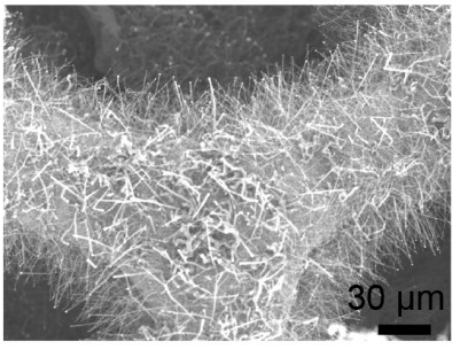

Figure S11. The SEM image of NSF/CNT sample after long-term OER.

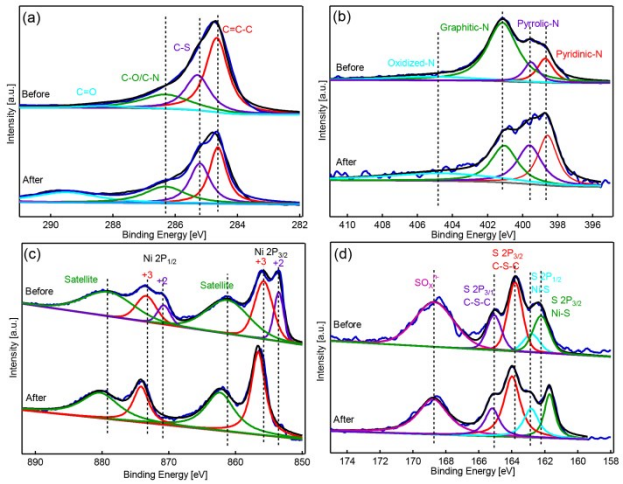

Figure S12. High resolution XPS (a) C 1s, (b) N 1s, (c) Ni 2p and (4) S 2p spectra for NSF/CNT catalysts before and after OER.

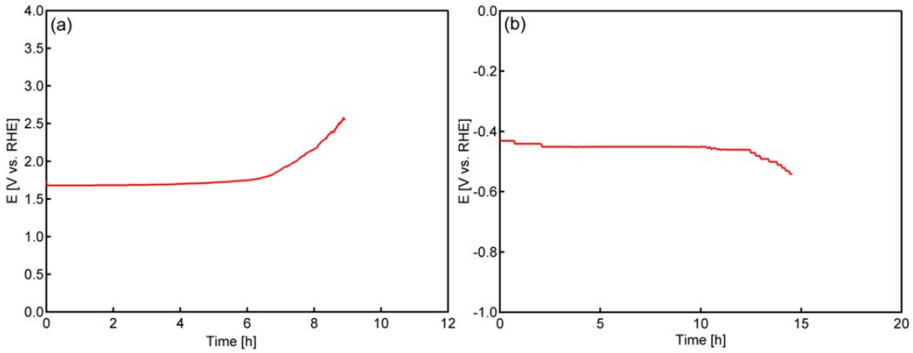

Figure S13. Long-term stability tests of the NSF as the working electrode for (a) OER and (b) HER at a current of 100 mA in N_2 saturated 1 M KOH.

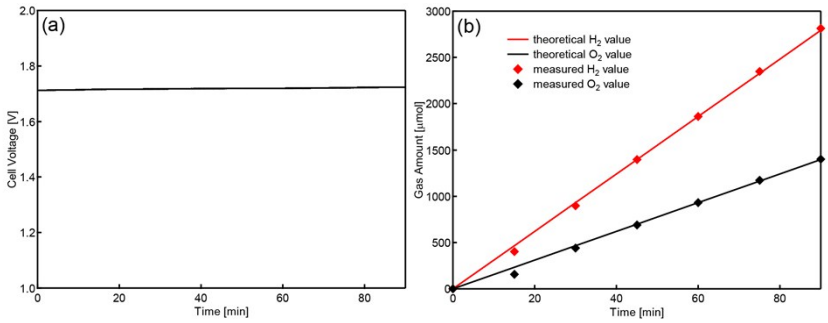

Figure S14. Performance of an overall water-splitting electrolyzer using NSF/CNT as electrocatalysts. (a) Chronopotential curve of water electrolysis using NSF/CNT as electrocatalyst for both HER and OER in a two-electrode configuration. (b) The time evolution of the amounts of theoretically calculated and experimentally determined oxygen (O_2) and hydrogen (H_2), which were produced during the water splitting process.

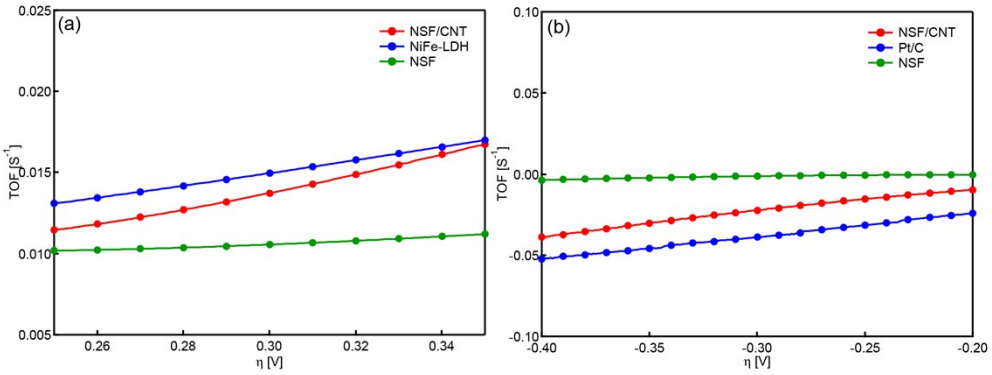

Figure S15. TOFs calculated at various potentials for (a) OER and (b) HER using different electrocatalysts.

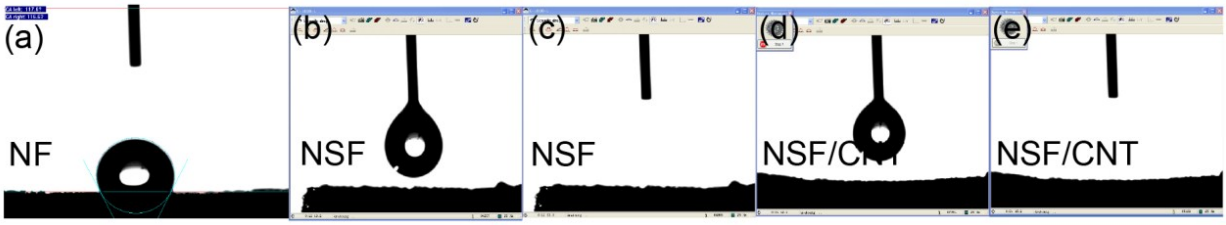

Figure S16. Hydrophilcity test of (a) Ni foam showing contact angle of 117°; (b,c) NSF showing contact angle of ~ 0°. (d,e) NSF/CNT showing contact angle of ~0°.

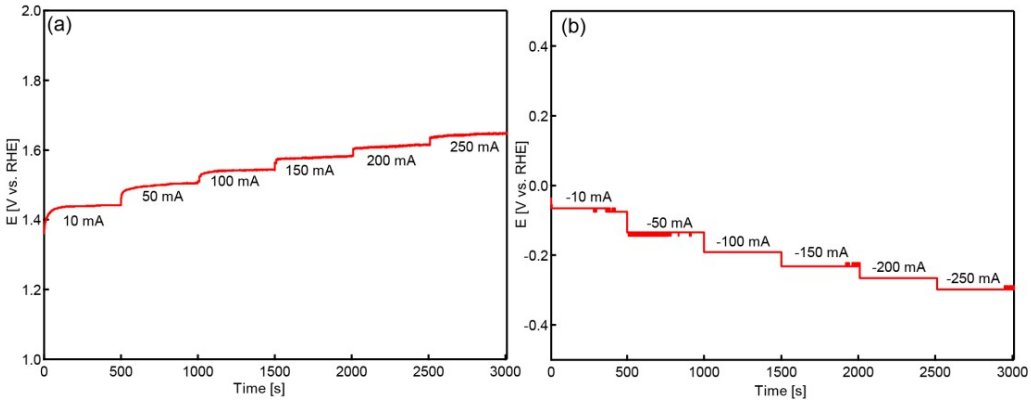

Figure S17. Multi-step current-time curves of NSF/CNT for (a)OER and (b) HER. The current density started at 10 mA/cm^2 and ended at 250 mA/cm^2, with an increment of 50 mA/cm^2 per 500 s.

Table S1. Comparison of the recently reported of highly active transition-metal-base bifunctional catalysts for both HER and OER in alkaline electrolyte. (Carbon Papers : CP ; Ni Foam : NF)

Bifunctional catalysts	Electrolyte	Substrate	η (mV) at j (mA cm^{-2})		Cell voltage (V) at j (mA cm^{-2})	Stability at j (mA cm^{-2})	Ref
			HER	OER			
MoS_2/Ni_3S_2	1.0 M KOH	NF	110@10	218@10	1.56@10	10h@10	5
Ni_3S_2	1.0 M KOH	CP	112@10	295@10	1.63@10	100h@10	6
Ni_3S_2 nanosheet	1.0 M KOH	NF	223@10	260@10	1.76@13	150h@10	7
N-Ni_3S_2	1.0 M KOH	NF	110@10	330@100	1.66@50	8h@20	8
$Fe_{11.1\%}$ -Ni_3S_2	1.0 M KOH	NF	203@50	234@50	1.66@20	42h@20	9

Co_9S_8/Ni_3S_2 nanowire	1.0 M KOH	NF	128@10	227@10	1.64@10	12h@10	10
NCT-$NiCo_2S_4$	1.0 M KOH	NF	295@100	330@100	1.6@10	15h@10	11
FeS_2/CoS_2	1.0 M KOH	NF	78.2@10	302@100	1.47@10	21h@15	12
Ni-Fe-Co-S nanosheets	1.0 M KOH	NF	215@100	272@100	1.54@10	10h@50	13
NiS_2 nanospheres	1.0 M KOH	CP	147@10	241@10	1.66@10	120 cycles	14
MoS_2/NiCoS nanosheets	1.0 M KOH	NF	189@10	290@10	1.5@10	22h@10	15
$Ni(OH)_2/Ni_3S_2$	1.0 M KOH	NF	211@20	270@20	1.57@10	500cycles	16
CuNiS NWs	1.0 M KOH	CP	71@10	307@30	1.54@10	25h@11	17
Se-(NiCo)S/OH	1.0 M KOH	NF	103@10	155@10	1.6@10	66h@10	18
N-C/NiS_2	1.0 M KOH	CP	78@10	264@10	1.63@30	48h@30	19
NSF/CNT	1.0 M KOH	NF	64@10 266@200	208@10 380@200	1.5@10 1.72@100	50h@100	This work

Reference for the SI:

1 Liu, J.; Wang, J.; Zhang, B.; Ruan, Y.; Lv, L.; Ji, X.; Jiang, J., Hierarchical $NiCo_2S_4$@ NiFe LDH heterostructures supported on nickel foam for enhanced overall-water-splitting activity. *ACS applied materials & interfaces* **2017**, *9* (18), 15364-15372.

2 Xu, W.; Lu, Z.; Sun, X.; Jiang, L.; Duan, X., Superwetting electrodes for gas-involving electrocatalysis. *Accounts of chemical research* **2018,** *51* (7), 1590-1598.

3 Wang, S.; Liu, K.; Yao, X.; Jiang, L., Bioinspired surfaces with superwettability: new insight on theory, design, and applications. *Chem. Rev.* **2015**, *115*, 8230-8293.

4 Derjaguin, B. V.; Muller, V. M.; Toporov, Y. P., Effect of contact deformations on the adhesion of particles. *J. Colloid Interface Sci.* **1975**, *53*, 314-326.

5 Zhang, J.; Wang, T.; Pohl, D.; Rellinghaus, B.; Dong, R.; Liu, S.; Feng, X., Interface engineering of MoS_2/Ni_3S_2 heterostructures for highly enhanced electrochemical overall-water-splitting activity. *Angewandte Chemie International Edition* **2016**, *55* (23), 6702-6707.

6 Zheng, X.; Han, X.; Zhang, Y.; Wang, J.; Zhong, C.; Deng, Y.; Hu, W., Controllable synthesis of nickel sulfide nanocatalysts and their phase-dependent performance for overall water splitting. *Nanoscale* **2019**, *11* (12), 5646-5654.

7 Feng, L. L.; Yu, G.; Wu, Y.; Li, G. D.; Li, H.; Sun, Y.; Zou, X., High-index faceted Ni_3S_2 nanosheet arrays as highly active and ultrastable electrocatalysts for water splitting. *Journal of the American Chemical Society* **2015**, *137* (44), 14023-14026.

8 Chen, P.; Zhou, T.; Zhang, M.; Tong, Y.; Zhong, C.; Zhang, N.; Xie, Y., 3D Nitrogen-Anion-Decorated Nickel Sulfides for Highly Efficient Overall Water Splitting. *Advanced Materials* **2017**, *29* (30), 1701584.

9 Zhu, W.; Yue, Z.; Zhang, W.; Hu, N.; Luo, Z.; Ren, M.; Wang, J., Wet-chemistry topotactic synthesis of bimetallic iron–nickel sulfide nanoarrays: an advanced and versatile catalyst for energy efficient overall water and urea electrolysis. *Journal of Materials Chemistry A* **2018**, *6* (10), 4346-4353.

10 Du, F.; Shi, L.; Zhang, Y.; Li, T.; Wang, J.; Wen, G.; Zou, Z., Foam–like Co_9S_8/Ni_3S_2 heterostructure nanowire arrays for efficient bifunctional overall water–splitting. *Applied Catalysis B: Environmental* **2019**, *253*, 246-252.

11 Li, F.; Xu, R.; Li, Y.; Liang, F.; Zhang, D.; Fu, W. F.; Lv, X. J., N-doped carbon coated $NiCo_2S_4$ hollow nanotube as bifunctional electrocatalyst for overall water splitting. *Carbon* **2019**, *145*, 521-528.

12 Li, Y.; Yin, J.; An, L.; Lu, M.; Sun, K.; Zhao, Y. Q.; Xi, P., FeS_2/CoS_2 interface nanosheets as efficient bifunctional electrocatalyst for overall water splitting. *Small* **2018**, *14* (26), 1801070.

13 Darband, G. B.; Aliofkhazraei, M.; Hyun, S.; Rouhaghdam, A. S.; Shanmugam, S., Electrodeposition of Ni–Co–Fe mixed sulfide ultrathin nanosheets on Ni nanocones: a low-cost, durable and high performance catalyst for electrochemical water splitting. *Nanoscale* **2019**, *11* (35), 16621-16634.

14 Shi, X.; Ling, X.; Li, L.; Zhong, C.; Deng, Y.; Han, X.; Hu, W., Nanosheets assembled into nickel sulfide nanospheres with enriched Ni^{3+} active sites for efficient water-splitting and zinc–air batteries. *Journal of Materials Chemistry A* **2019**, *7* (41), 23787-23793.

15 Qin, C.; Fan, A.; Zhang, X.; Wang, S.; Yuan, X.; Dai, X., Interface engineering: few-layer MoS_2 coupled to a NiCo-sulfide nanosheet heterostructure as a bifunctional electrocatalyst for overall water splitting. *Journal of Materials Chemistry A* **2019**, *7*(48), 27594-27602.

16 Du, X.; Yang, Z.; Li, Y.; Gong, Y.; Zhao, M., Controlled synthesis of $Ni(OH)_2/Ni_3S_2$ hybrid nanosheet arrays as highly active and stable electrocatalysts for water splitting. *Journal of Materials Chemistry A* **2018**, *6*(16), 6938-6946.

17 Cao, D.; Cheng, D., One-pot synthesis of copper–nickel sulfide nanowires for overall water splitting in alkaline media. *Chemical Communications* **2019**, *55* (56): 8154-8157.

18 Hu, C.; Zhang, L.; Zhao, Z. J.; Li, A.; Chang, X.; Gong, J., Synergism of geometric construction and electronic regulation: 3D Se-$(NiCo)S_x/(OH)_x$ nanosheets for highly efficient overall water splitting. *Advanced Materials* **2018**, *30* (12), 1705538.

19 Zhang, D.; Mou, H.; Chen, L.; Xing, G.; Wang, D.; Song, C., Surface/interface engineering N-doped carbon/NiS_2 nanosheets for efficiently electrocatalytic H_2O splitting. *Nanoscale* **2020**.